INORGANIC CHEMISTRY FRONTIERS

RESEARCH ARTICLE

View Article Online
View Journal | View Issue

Cite this: *Inorg. Chem. Front.*, 2026, **13**, 1091

An eco-friendly self-powered X-ray detector based on a multi-layered double perovskite ferroelectric

Qi Gao,†[a] Kuanhai Li,†[a] Yingying Zheng,[a] Panpan Yu,*[a,b] Yunpeng Yao,[c] Zeng-Kui Zhu[a] and Junhua Luo *[a,b]

Received 25th September 2025,
Accepted 14th November 2025

DOI: 10.1039/d5qi01949d

rsc.li/frontiers-inorganic

Self-powered X-ray detectors based on lead halide perovskites (LHPs) have recently gained increased traction due to their low energy consumption and easy fabrication. However, the toxicity of lead in LHPs threatens human and environmental safety, which hinders their commercialization. Herein, an eco-friendly self-powered X-ray detector has been successfully fabricated using a multilayered double perovskite ferroelectric $(C_6H_5CH_2NH_3)_2CsAgBiBr_7$ (**1**). The intrinsic ferroelectric spontaneous polarization property (P_s = 3.19 μC cm^{-2}) in **1** generates an impressive polar photovoltage of 0.5 V, which provides an ideal driving force for exciton dissociation within the material, enabling X-ray detection without an external power source. The X-ray detector based on **1** shows a high sensitivity of 47.2 μC Gy^{-1} cm^{-2} and an extremely low X-ray detection limit of 716 nGy s^{-1} at 0 V bias. Additionally, under an applied bias of 50 V, the sensitivity increases to 1154.8 μC Gy^{-1} cm^{-2}, surpassing that of most halide double perovskite detectors. This work sheds light on the great potential of multilayered double perovskite ferroelectrics for cost-effective "green" self-powered X-ray detectors.

1. Introduction

X-ray detectors which can convert X-rays into electrical signals play an indispensable role in many important fields, such as medical diagnosis, industrial production, and aerospace research.[1–3] Currently, commercial X-ray detectors mainly rely on pure inorganic semiconductors, such as Si, α-Se, CdTe, *etc*.[4–6] These materials still face some problems such as low X-ray absorption coefficients and huge energy costs for high-temperature fabrication processing, which stimulates the exploration of new material systems for high-performance X-ray detection. Recently, two-dimensional (2D) lead halide perovskites (LHPs) have gained a lot of attention as prominent candidate materials for X-ray detection due to their ease of fabrication, superior X-ray absorption, and exceptional optoelectronic properties.[7–9] For instance, (DGA)PbI_4 (DGA = dimethylbiguanide) achieves a prominent sensitivity of 4869 μC Gy^{-1} cm^{-2} with an ultralow dark current drift (I_{drift}) of 5.97 × 10^{-7} nA cm^{-1} s^{-1} V^{-1} by applying an external electric field of 1200 V mm^{-1}.[10] However, conventional detectors generally require external electric field application during operation, resulting in high energy consumption and complicated circuit systems that limit their practical application.[11,12] Therefore, exploring self-powered devices for high-performance X-ray detection without external bias is currently a research hotspot.[13–18]

Ferroelectric materials, which exhibit a bulk photovoltaic effect (BPVE) due to their inherent spontaneous polarization (P_s), are considered ideal candidates for self-powered X-ray detectors. Compared to materials with a central structure, this BPVE endows the material with a unique intrinsic electric field that promotes the independent separation of photo-excited charge carriers, thereby enabling X-ray detection without an external power source.[19–25] For example, the 2D perovskite ferroelectric $(CH_3OC_3H_9N)_2CsPb_2Br_7$ exhibited a notable sensitivity of 410 μC Gy^{-1} cm^{-2} under zero bias.[24] Despite the widespread recognition of lead-based ferroelectrics for their excellent optoelectronic properties, the inherent toxicity of Pb seriously threatens the human body and ecosystem. Therefore, exploring lead-free perovskite ferroelectrics with a strong BPVE is of significant importance for achieving prominent and eco-friendly self-powered X-ray detectors. The successful application of the double perovskite $(R\text{-MPA})_4AgBiI_8$ (*R*-MPA = *R*-β-methylphenethylammonium) on self-driven X-ray detectors suggests the huge potential of lead-free halide double perovskites (HDPs) for passive X-ray detectors.[19] At present, there are only a few reports on lead-free HDP ferroelectrics that achieve self-driven X-ray detectors, especially in multilayered lead-free HDPs. In general, the charge transport properties increase with the number of inorganic layers. Therefore, it is necessary to

[a]*Jiangxi Normal University, School of Chemical Engineering, Nanchang, Jiangxi 330022, China. E-mail: luojunhua@jxnu.edu.cn, ppyu@jxnu.edu.cn*
[b]*Fujian Institute of Research on the Structure of Matter, Chinese Academy of Sciences, State Key Laboratory of Structural Chemistry, Fuzhou, Fujian 350002, China*
[c]*Yantai University, School of Environmental and Material Engineering, Yantai 264005, P. R. China*
†These authors contributed equally to this work.

explore the potential of multilayered lead-free HDPs in application in self-driven X-ray detectors.

Herein, we successfully constructed an eco-friendly self-powered X-ray detector using the multilayered hybrid perovskite ferroelectric $(C_6H_5CH_2NH_3)_2CsAgBiBr_7$ (**1**). Owing to the remarkable spontaneous polarization in **1**, the BPVE was induced to separate the charge carriers, yielding a polar photovoltage of approximately 0.5 V. This built-in field gradient facilitates efficient photocarrier dissociation and directional transport, enabling a remarkable sensitivity of 47.2 μC Gy^{-1} cm^{-2} and a low limit of detection (LoD) of 716 nGy s^{-1} without external bias. External voltage enhances charge collection efficiency, further improving sensitivity to 1154.8 μC Gy^{-1} cm^{-2} at 50 V. This work demonstrated the great potential of multilayered lead-free layered perovskites for manufacturing X-ray detectors and provided a reliable pathway for fabricating eco-friendly self-powered X-ray detectors.

2. Results and discussion

High-quality orange single crystals (SCs) of compound **1** were prepared from saturated hydrobromic solutions by adding a certain proportion of Cs_2CO_3, Ag_2O, Bi_2O_3 and benzylamine *via* a slow cooling process (Fig. 1a). As shown in Fig. 1b and c, the scanning electron microscopy (SEM) and atomic force microscopy (AFM) images of **1** SC show a very flat and smooth morphology, which is important for carrier transport in self-powered X-ray detectors. As shown in Fig. 1d, the powder X-ray diffraction (PXRD) pattern of **1** is highly consistent with the simulated PXRD pattern from the crystal structure (CCDC 2010350),[26] verifying the phase purity. A pair of reversible peaks were observed in differential scanning calorimetry (DSC) measurements, indicating that a reversible phase transition occurred at 475 K for **1** (Fig. 1e). Furthermore, the thermodynamic stability of **1** was investigated by thermogravimetric analysis (TG), which revealed excellent thermal stability with a decomposition temperature as high as 570 K (Fig. S1). Fig. 1f shows that **1** adopts a typical Ruddlesden–Popper structure where alternating corner-sharing $[AgBr_6]^{5-}$ and $[BiBr_6]^{3-}$ octahedral units form the inorganic layers and the organic cations are firmly linked with the inorganic layers *via* N–H···Br interactions (2.89–3.12 Å). The spontaneous polarization was calculated to be 3.19 μC cm^{-2} along the polar axis (Fig. S2), resulting in the generation of the BPVE. The powerful BPVE provides further support for self-powered X-ray detection. Meanwhile, the piezoelectric response of **1** SC was tested along the direction perpendicular to the polar axis, and the test results

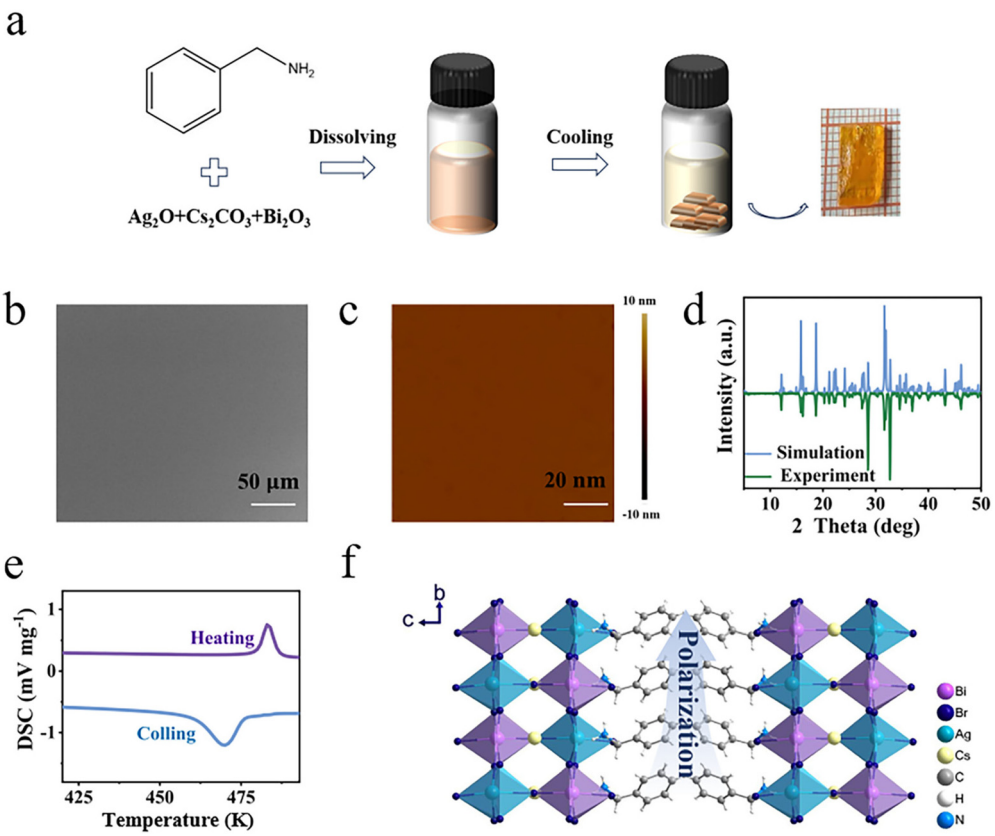

Fig. 1 (a) Schematic for the growth and a photograph of **1** SC. (b and c) SEM and AFM images of the surface of **1** SC, respectively. (d) The simulated and experimental powder XRD patterns of **1**. (e) DSC curve of **1**. (f) Crystal structure of **1** at room temperature, showing a spontaneous electric polarization along the polar *b*-axis.

further confirmed the polar axis to be in the *b*-axis direction (Fig. S3). Ultraviolet-visible (UV-vis) absorption spectroscopy reveals that the obvious absorption edge of **1** was observed at 533 nm (Fig. S4), where the optical bandgap of **1** was determined to be approximately 2.42 eV by using the *Tauc* plot. The current density–voltage curve along the *b*-axis further demonstrates that the bulk resistivity (ρ) of **1** is as high as 5.66×10^{10} Ω cm (Fig. S5). This value is comparable to that of other 2D HDPs, such as $(BA)_2CsAgBiBr_7$ (1.5×10^{11} Ω cm),[27] $(I\text{-}C_4H_8NH_3)_4AgBiI_8$ (3.04×10^{10} Ω cm)[28] and commercial CdZnTe (10^{10} Ω cm).[29] Notably, this resistivity is more than two orders of magnitude higher than that of conventional 3D $MAPbX_3$ (X = Cl, Br, I) perovskite SCs (10^7–10^8 Ω cm).[30–33] The exceptionally high resistivity of **1** contributes to its remarkably low dark current, suggesting that it holds significant potential as an effective material for X-ray detection.

X-ray absorption is an important parameter for X-ray detection. Therefore, we investigate our detector's X-ray absorption capacity by simulating the absorption efficiency across a broad photon energy range based on a photon cross-section database.[34] As depicted in Fig. 2a, **1** exhibits strong X-ray absorption across a wide photon energy range, surpassing that of Si and closely matching that of α-Se. This high absorption capability stems from the presence of heavy atoms such as Ag, Bi and Br. Due to density differences, the absorption coefficient of **1** (2.920 g cm^{-3}) is greater than that of $(BZA)_4AgBiBr_8$ (2.159 g cm^{-3}) but slightly lower than that of $Cs_2AgBiBr_6$ (4.93 g cm^{-3}).[35,36] Fig. 2b presents the relationship between attenuation efficiency and material thickness when the energy of X-ray photons reaches 50 keV. At a thickness of 2 mm, ferroelectric **1** attenuates approximately 95.8% of incident X-ray photons, significantly outperforming Si (23.4%). Based on its outstanding semiconducting properties and high X-ray absorption efficiency, **1** is believed to be a promising candidate for X-ray detectors. A two-terminal device was fabricated by depositing Ag electrodes on the surface of **1** along the direction of polarization (*b* axis), as illustrated in the inset of Fig. 2c. The mobility-lifetime product ($\mu\tau$), which reflects the efficiency of charge collection, is another key merit for X-ray detectors. The $\mu\tau$ is estimated by fitting current–voltage (*I*–*V*) characteristics under the exposure of X-rays using Hecht's equation. As shown in Fig. 2c, the $\mu\tau$ of **1** is calculated to be 1.3×10^{-3} cm^2 V^{-1}, which is 10^4 times higher than that of α-Se (~10^{-7} cm^2 V^{-1}) and higher than the reported values of $(BZA)_2(R/S\text{-}PPA)BiI_6$ (5.94×10^{-5} cm^2 V^{-1}), $(R\text{-}MPA)_4AgBiI_8$ (2.2×10^{-5} cm^2 V^{-1}), and $(HIA)_2AgBiBr_8$ (1.23×10^{-3}).[19,21,37] A pronounced BPVE along the direction of polarization is observed during *I*–*V* measurements because of the spontaneous polarization of **1** at room temperature. It can be observed that **1** shows an open-circuit voltage of 0.5 V under X-ray irradiation in Fig. 2d. Considering its strong X-ray absorption, excellent charge transport properties and significant BPVE, we conclude that **1** holds promising prospects for next-generation eco-friendly self-powered X-ray detectors.

To further investigate the X-ray detection performance of the **1** SC-based detectors, the photocurrent under X-ray

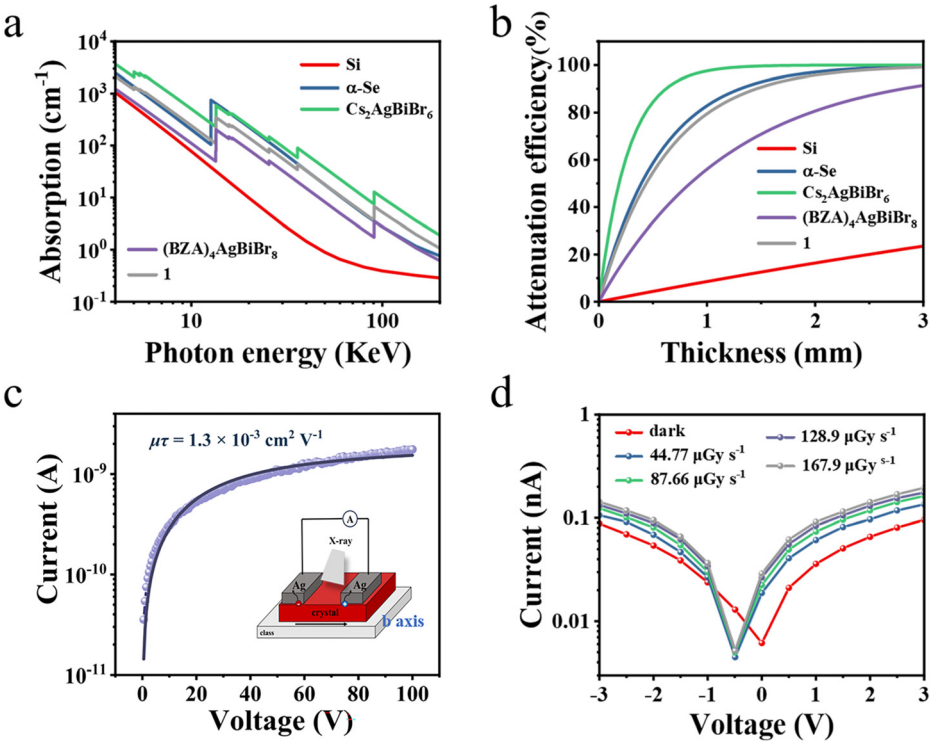

Fig. 2 (a) X-ray absorption spectra and (b) corresponding attenuation efficiencies of Si, α-Se, $Cs_2AgBiBr_6$, $(BZA)_4AgBiBr_8$, and **1**. (c) Bias-dependent X-ray conductivity of the **1** SC device. (d) *I*–*V* curves of the **1** device along the *b*-axis in the dark and under X-ray irradiation.

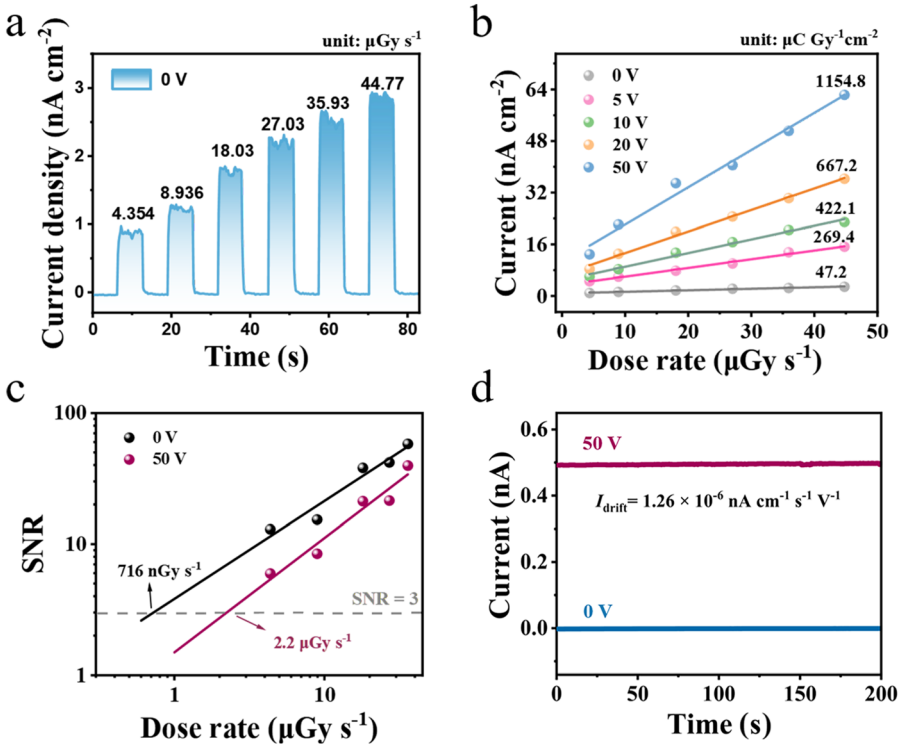

Fig. 3 (a) Current density–time curves of the **1** SC detector under increased X-ray dose rates at 0 V bias. (b) X-ray-induced current densities as a function of dose rates with external voltages increasing from 0 to 50 V. The slope of the fitting line represents the sensitivity. (c) SNRs of the **1** detector under different dose rates at 0 and 50 V bias. (d) Dark current drift under 0 and 50 V bias, respectively.

irradiation at different external voltages was measured. Notably, due to the pronounced BPVE generated by spontaneous polarization, the device demonstrates a strong response to X-rays even in the absence of an external bias (Fig. 3a). Notably, **1** exhibited a low dark current density (J_d) of approximately 10^{-11} A cm^{-2}, resulting from the high bulk resistivity. Such low J_d lays a solid foundation for high-performance X-ray detectors. As illustrated in Fig. 3a, the photocurrent density (J_{ph}) exhibits a nearly perfect linear increase as the X-ray dose rate rises from 4.35 to 44.77 μGy s^{-1}. The sensitivity was calculated to be 47.2 μC Gy^{-1} cm^{-2} under 0 V bias by fitting the relationship between the current density (J_{ph}–J_d) and dose rate (Fig. 3b). This value not only competes with commercial α-Se (20 μC Gy^{-1} cm^{-2}), which needs an exceptionally high electric field of 10 μm V^{-1}, but also significantly surpasses many lead-free perovskites operating at an applied voltage, such as $(CPA)_4AgBiBr_8$ (0.8 μC Gy^{-1} cm^{-2}, 10 V),[38] $(BA)_2CsAgBiBr_7$ (4.2 μC Gy^{-1} cm^{-2}, 10 V),[27] and $(HIA)_2AgBiI_8$ (118 μC Gy^{-1} cm^{-2}, 10 V).[9] Additionally, the X-ray responses to the dose rate of **1** under varying bias from 5 to 50 V were investigated (Fig. S6–S9). As expected, the sensitivity increases with increasing external electric fields due to enhanced charge collection efficiency, reaching a peak value of 1154.8 μC Gy^{-1} cm^{-2} at 50 V (Fig. 3b and Table S1). This value surpasses those of most of the HDP detectors and is even comparable to that of the widely known $Cs_2AgBiBr_6$ single-crystal detector.[39] LoD is defined as the lowest dose rate where the signal-to-noise ratio (SNR) equals 3, a critical metric for evaluating X-ray detectors' performance. The plot of SNR *versus* dose rate is presented in Fig. 3c. By linearly fitting the function of SNR and the dose rate, the LoD of **1** is calculated to be 716 nGy s^{-1} at 0 V bias. It should be noticed that this value is much lower (about 7.6 times) than the standard dose rate (5.5 μGy s^{-1}) used in medical imaging. When the external bias is enhanced to 50 V, the LoD increases to 2.2 μGy s^{-1}, which is attributed to the amplified dark current and noise arising from significant ion migration under high electric fields. Ion migration was further assessed through current drift (I_{drift}). Under self-powered operation, the dark current remains exceptionally stable due to negligible ion migration. In contrast, at 50 V bias, I_{drift} reaches 1.26 × 10^{-6} nA cm^{-1} s^{-1} V^{-1}, highlighting the unique virtue of self-powered mode in operational stability (Fig. 3d). The radiation stability was further evaluated by measuring the photocurrent of the **1** SC-based detector under continuous X-ray exposure at a dose rate of 1.99 mGy s^{-1}. It is remarkable that after a large amount of X-ray dose irradiation, both dark current and photocurrent at 0 V and 50 V bias remained ultra stable (Fig. S10), suggesting the excellent irradiation stability of the **1** SC device. Taking all these advantages into account, the **1** SC-based X-ray detector outperforms most reported HDP detectors and is even comparable to some reported devices, as summarized in Table S1.

3. Conclusion

In summary, we have successfully achieved eco-friendly self-powered X-ray detection based on a 2D multilayered double perovskite ferroelectric. Combining the strong BPVE induced by ferroelectric spontaneous polarization with excellent radiation absorption ability, the X-ray detectors based on **1** SC achieve a high sensitivity of 47.2 μC Gy^{-1} cm^{-2}, an ultralow LoD of 716 nGy s^{-1} and remarkable operational stability under zero bias. Furthermore, when an external bias reaches 50 V, the sensitivity is significantly enhanced to a maximum of 1154.8 μC Gy^{-1} cm^{-2}, surpassing most previously reported HDP detectors. This study not only demonstrates the huge potential of HDPs on self-powered X-ray detection but also provides valuable insights into the development of next-generation "green" self-powered X-ray detectors.

Author contributions

Q. Gao, K. H. Li, and Y. Y. Zheng prepared the samples, performed data collation, and wrote the manuscript. Q. Gao and K. H. Li carried out the X-ray performance testing. Y. P. Yao and Z.-K. Zhu provided assistance with single crystal analysis. P. P. Yu and J. H. Luo designed and directed this project. All the authors discussed and commented on the manuscript.

Conflicts of interest

There are no conflicts to declare.

Data availability

The data supporting the findings of this study are available in the supplementary information (SI). Supplementary information including experimental section, extra experimental data, additional X-ray detection performance, and summary of some reported perovskite-based X-ray detectors is available. See DOI: **https://doi.org/10.1039/d5qi01949d**.

Acknowledgements

This work was financially supported by the National Natural Science Foundation of China (22435005, 22193042, 22201284, 22305105, 22125110, 22122507, and U21A2069), the Jiangxi Provincial Natural Science Foundation (20252BAC200222, 20242BAB25129, and 20224BAB213003), the Natural Science Foundation of Fujian Province (2023J05076), and the Jiangxi Provincial Education Department Science and Technology Research Foundation (GJJ2200384), Natural Science Foundation of Shandong Province (ZR2023QB005).

References

1 Y. C. Kim, K. H. Kim, D. Y. Son, D. N. Jeong, J. Y. Seo, Y. S. Choi, I. T. Han, S. Y. Lee and N. G. Park, Printable organometallic perovskite enables large-area, low-dose X-ray imaging, *Nature*, 2017, **550**, 87.
2 H. D. Wu, Y. S. Ge, G. D. Niu and J. Tang, Metal halide perovskites for X-ray detection and imaging, *Matter*, 2021, **4**, 144–163.
3 G. H. Dun, H. N. Zhang, K. Qin, X. C. Tan, R. Zhao, M. Chen, Y. Huang, X. S. Geng, Y. Y. Li and Y. H. Li, Wafer-scale photolithography-pixeled Pb-free perovskite X-ray detectors, *ACS Nano*, 2022, **16**, 10199–10208.
4 G. Rikner and E. Grusell, Effects of radiation damage on p-type silicon detectors, *Phys. Med. Biol.*, 1983, **28**, 1261–1267.
5 S. O. Kasap, X-ray sensitivity of photoconductors: application to stabilized α-Se, *J. Phys. D: Appl. Phys.*, 2000, **33**, 2853–2865.
6 M. Fiederle, S. Procz, E. Hamann, A. Fauler and C. Frojdh, Overview of GaAs und CdTe pixel detectors using Medipix electronics, *Cryst. Res. Technol.*, 2020, **55**, 2000021.
7 Y. Wu, Z. Yang, Y. C. Liu and S. Z. Liu, Halide perovskite: a promising candidate for next–generation X–ray detectors, *Adv. Sci.*, 2022, **10**, 2205536.
8 J. L. Peng, C. Q. Xia, Y. L. Xu, R. M. Li, L. H. Cui, J. K. Clegg, L. M. Herz, M. B. Johnston and Q. Q. Lin, Crystallization of $CsPbBr_3$ single crystals in water for X-ray detection, *Nat. Commun.*, 2021, **12**, 1531.
9 N. Fiuza-Maneiro, K. Sun, I. Lopez-Fernandez, S. Gomez-Grana, P. Muller-Buschbaum and L. Polavarapu, Ligand Chemistry of Inorganic Lead Halide Perovskite Nanocrystals, *ACS Energy Lett.*, 2023, **8**, 1152–1191.
10 B. B. Zhang, T. Zheng, J. X. You, C. Ma, Y. C. Liu, L. Zhang, J. Xi, G. H. Dong, M. Liu and S. Z. Liu, Electron–phonon coupling suppression by enhanced lattice rigidity in 2D perovskite single crystals for high–performance X–Ray detection, *Adv. Mater.*, 2023, **35**, 2208875.
11 X. W. Xu, W. Qian, S. Xiao, J. Wang, S. Z. Zheng and S. H. Yang, Halide perovskites: A dark horse for direct X–ray imaging, *EcoMat*, 2020, **2**, e12064.
12 B. Xiao, Q. H. Sun, F. B. Wang, S. Y. Wang, B. B. Zhang, J. J. Wang, W. Q. Jie, P. Sellin and Y. D. Xu, Towards superior X-ray detection performance of two-dimensional halide perovskite crystals by adjusting the anisotropic transport behavior, *J. Mater. Chem. A*, 2021, **9**, 13209–13219.
13 X. J. Zheng, W. Zhao, P. Wang, H. R. Tan, M. I. Saidaminov, S. J. Tie, L. G. Chen, Y. F. Peng, J. D. Long and W. H. Zhang, Ultrasensitive and stable X-ray detection using zero-dimensional lead-free perovskites, *J. Energy Chem.*, 2020, **49**, 299–306.
14 B. Shabbir, J. C. Yu, T. Warnakula, R. A. W. Ayyubi, J. A. Pollock, M. M. Hossain, J. E. Kim, N. Macadam, L. W. T. Ng and T. Hasan, Printable Perovskite Diodes for Broad–Spectrum Multienergy X–Ray Detection, *Adv. Mater.*, 2023, **35**, 2210068.

15 C. Ma, F. Chen, X. Song, M. Chen, L. L. Gao, P. J. Wang, J. L. Wen, Z. Yang, Y. Z. Tang and K. Zhao, Centimeter–sized molecular perovskite crystal for efficient X–ray detection, *Adv. Funct. Mater.*, 2021, **31**, 2100691.
16 Y. H. He, I. Hadar, M. C. De Siena, V. V. Klepov, L. Pan, D. Y. Chung and M. G. Kanatzidis, Sensitivity and Detection Limit of Spectroscopic–Grade Perovskite $CsPbBr_3$ Crystal for Hard X–Ray Detection, *Adv. Funct. Mater.*, 2022, **32**, 2112925.
17 X. He, M. L. Xia, H. D. Wu, X. Y. Du, Z. H. Song, S. Zhao, X. Chen and G. D. Niu, Quasi–2D perovskite thick film for X–ray detection with low detection limit, *Adv. Funct. Mater.*, 2021, **32**, 2109458.
18 F. Sun, H. Xu, W. Hong, Z. Sun and W. Liu, 2D $CuInP_2Se_6$ in High–Sensitivity UV–vis And X–Ray Detection, *Adv. Funct. Mater.*, 2024, **34**, 2313776.
19 J. B. Wu, S. H. You, P. P. Yu, Q. W. Guan, Z. K. Zhu, Z. Li, C. Qu, H. Q. Zhong, L. A. Li and J. H. Luo, Chirality Inducing Polar Photovoltage in a 2D Lead-Free Double Perovskite toward Self-Powered X-ray Detection, *ACS Energy Lett.*, 2023, **8**, 2809–2816.
20 S. H. You, Z. K. Zhu, S. H. Dai, J. B. Wu, Q. W. Guan, T. T. Zhu, P. P. Yu, C. J. Chen, Q. S. Chen and J. H. Luo, Inch–Size Single Crystals of Lead–Free Chiral Perovskites with Bulk Photovoltaic Effect for Stable Self–Driven X–Ray Detection, *Adv. Funct. Mater.*, 2023, **33**, 2303523.
21 Z. K. Zhu, T. T. Zhu, J. B. Wu, Y. Zeng, Q. W. Guan, Z. Li, C. Qu, H. Q. Zhong, L. N. Li and J. H. Luo, Chiral–Achiral Cations Intercalation Induced Lead–Free Chiral–Polar Hybrid Perovskites Enable Self–Powered X–Ray and Ultraviolet–Visible–Near–Infrared Photo Detection, *Small*, 2023, **20**, 2307454.
22 I. H. Park, K. C. Kwon, Z. Y. Zhu, X. Xu, R. L. Li, Q. H. Xu and K. P. Loh, Self-powered photodetector using two-dimensional ferroelectric Dion–Jacobson hybrid perovskites, *J. Am. Chem. Soc.*, 2020, **142**, 18592–18598.
23 P. J. Huang, K. Taniguchi and H. Miyasaka, Bulk photovoltaic effect in a pair of chiral–polar layered perovskite-type lead iodides altered by chirality of organic cations, *J. Am. Chem. Soc.*, 2019, **141**, 14520–14523.
24 C. M. Ji, Y. Z. Li, X. T. Liu, Y. X. Wang, T. T. Zhu, Q. Chen, L. Li, S. Wang and J. H. Luo, Monolayer-to-Multilayer Dimensionality Reconstruction in a Hybrid Perovskite for Exploring the Bulk Photovoltaic Effect Enables Passive X-ray Detection, *Angew. Chem.*, 2021, **133**, 21138–21144.
25 C. M. Ji, S. S. Wang, Y. X. Wang, H. X. Chen, L. N. Li, Z. H. Sun, Y. Sui, S. A. Wang and J. H. Luo, 2D hybrid perovskite ferroelectric enables highly sensitive X–ray detection with low driving voltage, *Adv. Funct. Mater.*, 2019, **30**, 1905529.
26 Y. P. Yao, H. D. Jiang, Y. Peng, X. Y. Zhang, S. Chen, X. T. Liu and J. H. Luo, High-curie temperature multilayered hybrid double perovskite photoferroelectrics induced by aromatic cation alloying, *J. Am. Chem. Soc.*, 2021, **143**, 15900–15906.
27 Z. Y. Xu, X. Liu, Y. B. Li, X. T. Liu, C. M. Ji, S. G. Han, Y. D. Xu and J. H. Luo, Exploring Lead-Free Hybrid Double Perovskite Crystals of $(BA)_2CsAgBiBr_7$ with Large Mobility-Lifetime Product toward X-Ray Detection, *Angew. Chem.*, 2019, **131**, 15904–15908.
28 Z. J. Zhu, H. J. Wu, D. Li, W. T. Wu, L. N. Li and J. H. Luo, A lead-free I-based hybrid double perovskite $(IC_4H_8NH_3)_4AgBiI_8$ for X-ray detection, *J. Mater. Chem. C*, 2021, **9**, 13157–13161.
29 Q. H. Sun, B. Z. Ge, B. Xiao, F. P. Li, L. L. Li, Z. Yin, J. Guo, J. Tang, C. J. Zhou, W. Q. Jie, M. H. Zhu and Y. D. Xu, High-Performance Industrial-Grade $CsPbBr_3$ Single Crystal by Solid–Liquid Interface Engineering, *Adv. Sci.*, 2023, **10**, 2302236.
30 W. L. Yu, F. Li, M. R. Niazi, Y. T. Xou, D. Corzo, A. Basu, C. Ma, S. Dey and M. L. Tietze, Single crystal hybrid perovskite field-effect transistors, *Nat. Commun.*, 2018, **9**, 5354.
31 R. Munir, A. D. Sheikh, M. Abdelsamie, H. Hu, L. Y. Yu, K. Zhao, T. Kim, O. E. Tall, R. P. Li, D. M. Smilgies and A. Amassian, Direct-write optical patterning of P3HT films beyond the diffraction limit, *Adv. Mater.*, 2017, **29**, 1603221.
32 F. T. Li, J. F. Lu, Q. L. Zhang, D. F. Peng, Z. Yang, Q. Xu, C. F. Pan, A. L. Pan, T. F. Li and R. M. Wang, Controlled fabrication, lasing behavior and excitonic recombination dynamics in single crystal $CH_3NH_3PbBr_3$perovskite cuboids, *Sci. Bull.*, 2019, **64**, 698–704.
33 Z. Y. Deng, F. X. Wei, S. J. Sun, G. Kieslich, A. K. Cheetham and P. D. Bristowe, Exploring the properties of lead-free hybrid double perovskites using a combined computational-experimental approach, *J. Mater. Chem. A*, 2016, **4**, 12025–12029.
34 G. Chen, Z.-K. Zhu, J. Wu, P. Yu, Y. Zeng, H. Dai, H. Yang, H. Wu, Y. Wang and J. H. Luo, Structural Reconfiguration via Alternating Cation Intercalation of Chiral Hybrid Perovskites for Efficient Self-Driven X-ray Detection, *ACS Appl. Mater. Interfaces*, 2024, **16**, 67970–67978.
35 P. Xu, H. Ye, Y. P. Yao, T. T. Zhu and J. H. Luo, Lead–Free Double Perovskite Semiconductor with Rigid Spacer–Induced High–Tc Dielectric Switch Features, *Chem. – Eur. J.*, 2023, **29**, e202300667.
36 W. C. Pan, H. D. Wu, J. J. Luo, Z. Z. Deng, C. Ge, C. Chen, X. W. Jiang, W. J. Yin, G. D. Niu, L. J. Zhu, L. X. Yin, Y. Zhou, Q. G. Xie, X. X. Ke, M. L. Sui and J. Tang, $Cs_2AgBiBr_6$ single-crystal X-ray detectors with a low detection limit, *Nat. Photonics*, 2017, **11**, 726.
37 W. Q. Guo, H. J. Xu, Q. S. Fan, P. F. Zhu, Y. Ma, Y. Liu, X. Zeng, J. H. Luo and Z. H. Sun, Centimeter-Size Single Crystal of a Polar Dion–Jacobson Double Perovskite with Large Mobility-Lifetime Product toward Effective X-Ray Detection, *Adv. Opt. Mater.*, 2024, **12**, 2303291.
38 W. Q. Guo, X. T. Liu, S. G. Han, Y. Liu, Z. Y. Xu, M. C. Hong, J. H. Luo and Z. H. Sun, Room-Temperature Ferroelectric Material Composed of a Two-Dimensional Metal Halide Double Perovskite for X-ray Detection, *Angew. Chem., Int. Ed.*, 2020, **59**, 13879–13884.
39 H. W. Lei, D. Hardy and F. Gao, Lead-Free Double Perovskite $Cs_2AgBiBr_6$: Fundamentals, Applications, and Perspectives, *Adv. Funct. Mater.*, 2021, **31**, 210589.

